Origin of the tunable carrier selectivity of atomic-layer-deposited TiO_x nanolayers in crystalline silicon solar cells

Takuya Matsui[1,2,*], Martin Bivour[1], Paul F. Ndione[1,3], Ruy S. Bonilla[4], Martin Hermle[1]

[1]Fraunhofer Institute for Solar Energy Systems ISE, Heidenhofstrasse 2, Freiburg 79110, Germany

[2]National Institute of Advanced Industrial Science and Technology (AIST), 1-1-1 Umezono, Tsukuba, Ibaraki, 305-8568, Japan

[3]National Renewable Energy Laboratory, 15013 Denver West Parkway, Golden, CO 80401, USA

[4]Department of Materials, University of Oxford, Parks Rd, Oxford, OX1 3PH, United Kingdom

*E-mail: t-matsui@aist.go.jp

Abstract – Titanium oxide (TiO_x) nanolayers grown by atomic layer deposition are investigated with respect to their application as carrier selective contacts for crystalline silicon (c-Si) solar cells. Although TiO_x is known to act as an electron contact, in this work the selectivity of TiO_x layers is found to be widely tunable from electron to hole selective depending on deposition conditions, post-deposition treatments, and work function of the metal electrode used. Using TiO_x and an intrinsic hydrogenated amorphous silicon buffer layer, solar cell test structure exhibiting open-circuit voltages (V_{oc}) as high as 720 and 650 mV are shown for electron and hole selective contacts, respectively. Surface photovoltage and capacitance-voltage measurements reveal that carrier selectivity is correlated with the amount of c-Si band bending induced by TiO_x, which are governed not only by the effective work function difference at the Si/TiO_x interface, but also by the negative fixed charge present in the TiO_x layer. This new finding is in contrast to the previous model for carrier transport where selectivity is determined only by the asymmetric band offsets at the Si/contact interface. It highlights the influence of induced band bending to produce carrier depletion/inversion conditions, and the importance of its selectivity effect in a c-Si absorber.

Keywords: solar cells; carrier selective contacts; titanium oxide; atomic layer deposition.

1. Introduction

In crystalline silicon (c-Si) solar cells, the conventional *p-n* homojunction has been used for separating the majority and minority carrier transports towards the respective contacts. Nevertheless, the heavy doping in the emitter and back surface field (BSF) regions, and the lack of surface passivation in the metallized device regions give rise to an increase of recombination current, which in turn limits the open-circuit voltage (V_{oc}) and fill factor (FF) of solar cells. Carrier selective contacts, which extract one type of photogenerated carrier (electron or hole)

from the c-Si light absorber, are an alternative avenue to realize a device without additional doping in the c-Si.[1] The archetypal selective contact scheme is the well-known silicon heterojunction (SHJ) structure. Here, the intrinsic and doped hydrogenated amorphous silicon (a-Si:H) layers are deposited on c-Si, serving as excellent surface passivation and carrier selective contact, respectively. In fact, this ideal passivating contact has led to the several high performing c-Si solar cells.[2,3] Meanwhile, another passivating contact scheme based on a tunneling oxide/polycrystalline silicon (SiO_2/poly-Si) stack[4] has emerged, demonstrating efficiencies of 25.8%[5] and 26.1%.[6] Other approaches for which the hole or electron selectivity does not rely on *p*- or *n*-type doped silicon thin films use high or low work function contact materials.

Recently, various transition-metal oxides such as MoO_x,[7] WO_x,[8] V_2O_x [9] and NiO_x [10] have been demonstrated as transparent hole selective contacts for c-Si solar cells. The origin of the hole selectivity is attributed to their high work function that provides induced band bending at the c-Si surface so that holes in c-Si can be selectively extracted to the external circuit. On the other hand, efficient electron selective contacts have been less thoroughly studied. Some insulating low-work-function materials such as MgF,[11] MgO[12] and LiF[13] have been reported but deeper understanding is still lacking. TiO_x (or TiO_2) thin layers deposited by chemical vapor deposition (CVD) [14,15] and atomic layer deposition (ALD)[16-19] have also been reported to act as semiconducting electron selective contacts to crystalline silicon solar cells, enabling the full-area rear contact without complex electrode patterning. Yang *et al*. have reported a 22.1% efficient solar cell by applying a thermal-ALD TiO_x as a rear electron contact for *n*-type c-Si absorber.[20] The origin of the electron selectivity of TiO_x has been ascribed to the asymmetric current flow at the Si/TiO_x interface where the small conduction band offset allows the electron flow while the large valence band offset inhibits the hole flow.[14-16] The influence of the capping metal work function on the electron selectivity has been also reported.[20-25] Meanwhile, it has been argued that TiO_x grown by CVD and ALD contains

negative fixed charge.[26-28] Due to this charge, TiO_x has been applied to boron-doped emitter to take advantage of its field-effect passivation.[28] However, the presence of such negative charge might be detrimental in aiming for an effective electron selective contact. Thus, in-depth understanding of the TiO_x layers with respect to its application as carrier selective contact is still lacking, yet it is of prime importance to exploit the potential of this material. Most importantly, the carrier selectivity of TiO_x layer should be evaluated independent from its surface passivation, as both issues greatly influence the solar cell performance, particularly for V_{oc}.

In this work, we have studied the carrier selectivity of ALD TiO_x nanolayers using interface electrical characterization techniques. Two different oxidation processes using oxygen plasma and thermal reaction with H_2O vapor were employed to synthesize the layers. To focus on the ability of TiO_x as a carrier selective contact, an a-Si:H buffer layer was introduced at the c-Si and TiO_x interface to maintain the passivation quality. Our results show that the carrier selectivity of TiO_x is widely tunable from electron-selective (V_{oc}~720 mV) to hole-selective (V_{oc}~650 mV) by controlling the ALD process, post-deposition treatments, and the contact material that covers the TiO_x layer. The origin of the tunable carrier selectivity of TiO_x is discussed and found to relate to the measured induced band bending at the c-Si/TiO_x interface. These findings advance the current understanding not only of TiO_x as a passivating selective contact, but also of other metal oxide layers currently under intensive research. Furthermore, these results constitute an important step forward in the interface engineering of high performance, full area, passivating and selective contacts for silicon solar cells.

2. Experimental

2.1. ALD process for TiO_x deposition

TiO_x layers were deposited on c-Si by an ALD system (FlexAL, Oxford Instruments) using titanium isopropoxide (TTIP) as a Ti precursor at a substrate temperature of 200 °C. Ar

was chosen as a carrier gas and a purge gas. The oxidation during every ALD cycle took place using either O_2 plasma or thermal reaction with H_2O vapor. We term these processes as plasma- and thermal-ALD, respectively. In the plasma-ALD process, O_2 plasma was generated by a remote inductively-coupled plasma (ICP) source. The plasma power was 300 W and the O_2 pressure was 15 mTorr. For thermal ALD process, H_2O vapor was introduced from the water pod whose temperature was kept at ~25 ºC. The H_2O dose was controlled by the valve opening time. In the steady state (>~1 s), the H_2O pressure in the process chamber was approximately 100 mTorr. The layer thickness and the optical properties of the deposited TiO_x were characterized by spectroscopic ellipsometry (J.A. Woollam) using the Tauc-Lorentz model. The native oxide layer of c-Si was not stripped off for this measurement in order to avoid the possible interfacial layer formation at the Si/TiO_x interface that might depend on the ALD condition.

2.2. Solar cell precursor fabrication and characterization

Shinny-etched c-Si wafers (*n*- or *p*-type float zone silicon, 1 Ωcm, (100) orientation, 200 μm thick) were RCA-cleaned and HF-dipped prior to deposition process. The front contact was formed using a standard SHJ structure (i.e., a-Si:H *i-p* or *i-n* stack) by plasma-enhanced chemical vapor deposition (PECVD), following a sputtered ITO layer.[8] For the rear contact, an intrinsic a-Si:H buffer layer (8-15 nm) was deposited prior to TiO_x. As a rear electrode after ALD-TiO_x, four different conductive materials (Ti, Al, Pd, and indium-tin oxide (ITO)) were examined. Then, samples were annealed at 180 °C for 15 min in ambient air. The carrier selectivity of plasma- and thermal-ALD TiO_x layers was characterized by measuring suns-V_{oc}[29] of the solar cell precursors, while the c-Si surface passivation was checked by measuring the quasi-steady state photoconductance (QSSPC) (Sinton WCT-120)[30] before the capping layer deposition at the rear.

2.3. Characterization of TiO_x

Apart from the solar cell precursors, TiO_x layers were directly deposited on (*n*)c-Si to evaluate their passivation ability by QSSPC. Prior to TiO_x deposition, the other side of the c-Si wafer was passivated by a-SiN_x:H layer grown by PECVD at >400 ºC. Furthermore, surface photovoltage (SPV) and capacitance-voltage (C-V) measurements were performed to investigate the TiO_x/c-Si interface properties. SPV measurement was applied to TiO_x layers deposited on (*n*) and (*p*)c-Si (1 Ωcm) to measure the induced c-Si band bending.[31,32] A 905 nm laser pulse was used as an excitation light source and illuminated through the TiO_x layer. Using above-mentioned TiO_x/(*n*)c-Si/a-SiN_x:H samples, C-V measurements were conducted on a Keysight E4980A LCR meter. A metal-insulator-semiconductor (MIS) structure was formed on the TiO_x layer by depositing ~50 nm of aluminum using thermal evaporation through a shadow mask to form front contacts. The contact area was measured using an optical microscope at ~50× magnification, calibrated using a standard checkboard pattern. For the samples reported here the area was 0.0123 cm^2. Rear contacts were formed using a Gallium-Indium eutectic after removing the a-SiN_x:H. Calculations of the insulation capacitance and flat-band voltage were not possible due to excessive leakage through the TiO_x layer, yet simulated C-V curves were calculated using the theory outlined by Nicollian and Brews.[33] For above characterizations, c-Si wafers were treated in a same manner prior to the layer deposition as for the solar cell precursors. However, c-Si wafers were not HF-dipped for SPV samples, as the native oxide layer does not affect much the SPV measurement.

3. Results

3.1. Film properties of ALD-TiO_x

TiO_x layers were deposited on c-Si to check the deposition rate and the optical properties. **Figure 1** shows the growth rate per cycle (GPC) of the TiO_x layers as a function of the oxidation time of either O_2 plasma or H_2O dose. In case of the plasma-ALD process, the GPC increases with oxidation time and reach the saturation of 0.045 nm at >4 s. This saturation of GPC is a

signature of an ideal ALD mode as it is a self-limiting deposition process. On the other hand, the GPC saturation of the thermal-ALD depends strongly on the Ar purge time (t_{purge}) after H_2O dose. If the t_{purge} is not long enough (e.g., 10 s), GPC increases without saturation and surpasses the theoretical limit of GPC that is determined by the molecular size of the precursor.[34] This indicates that a non-ideal gas-phase reaction takes place between the residual H_2O vapor and TTIP precursor. Accordingly, we used the least t_{purge} of 30 s, which is much longer than required for plasma-ALD (2 s), to perform deposition under proper ALD mode. This results in similar GPC between plasma- and thermal-ALD.

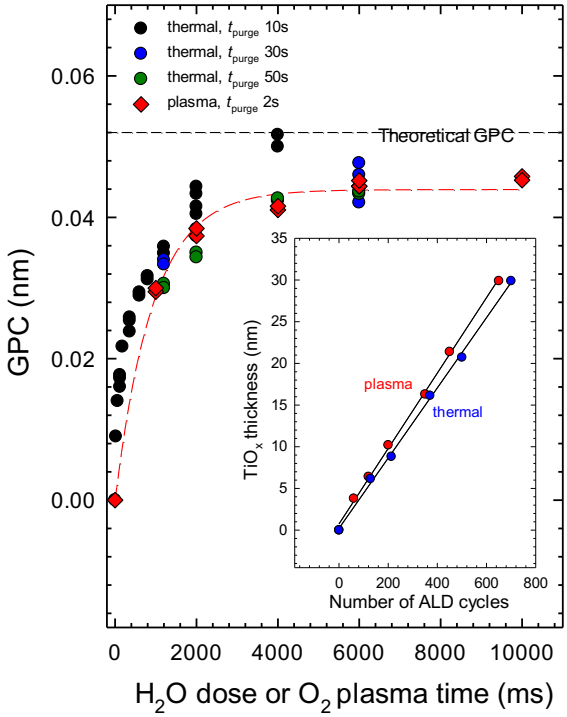

Figure 1. Growth rate per cycle (GPC) of the thermal- and plasma-ALD TiO_x films as a function of oxidation time (H_2O dose or O_2 plasma time) with different purge times (t_{purge}) after oxidation step. Inset shows the linear relationship between the TiO_x thickness and the number of ALD cycles for TiO_x films deposited under oxidation time of 6 s.

In terms of optical properties, the plasma-ALD always shows slightly higher refractive index over the whole range of wavelength compared to that of the thermal-ALD TiO_x (see Fig. S1, Supporting Information), although the measurement precision of the optical constant was

not thoroughly investigated. The TiO_x layers deposited by thermal-ALD using a different precursor ($TiCl_4$) have been reported to have n=2.39 at a wavelength of 632 nm,[35] which is close to our plasma-ALD TiO_x (n~2.4) but higher than our thermal-ALD TiO_x (n~2.3). These results indicate that thermal-ALD TiO_x has a less compact microstructure possibly due to the incorporation of H or H_2O in the film. The band gap of these TiO_x layers based on the Tauc-Lorenz model is about 3.4 eV, and their sub-band gap optical absorption (λ >370 nm) is negligibly low for solar cell application.

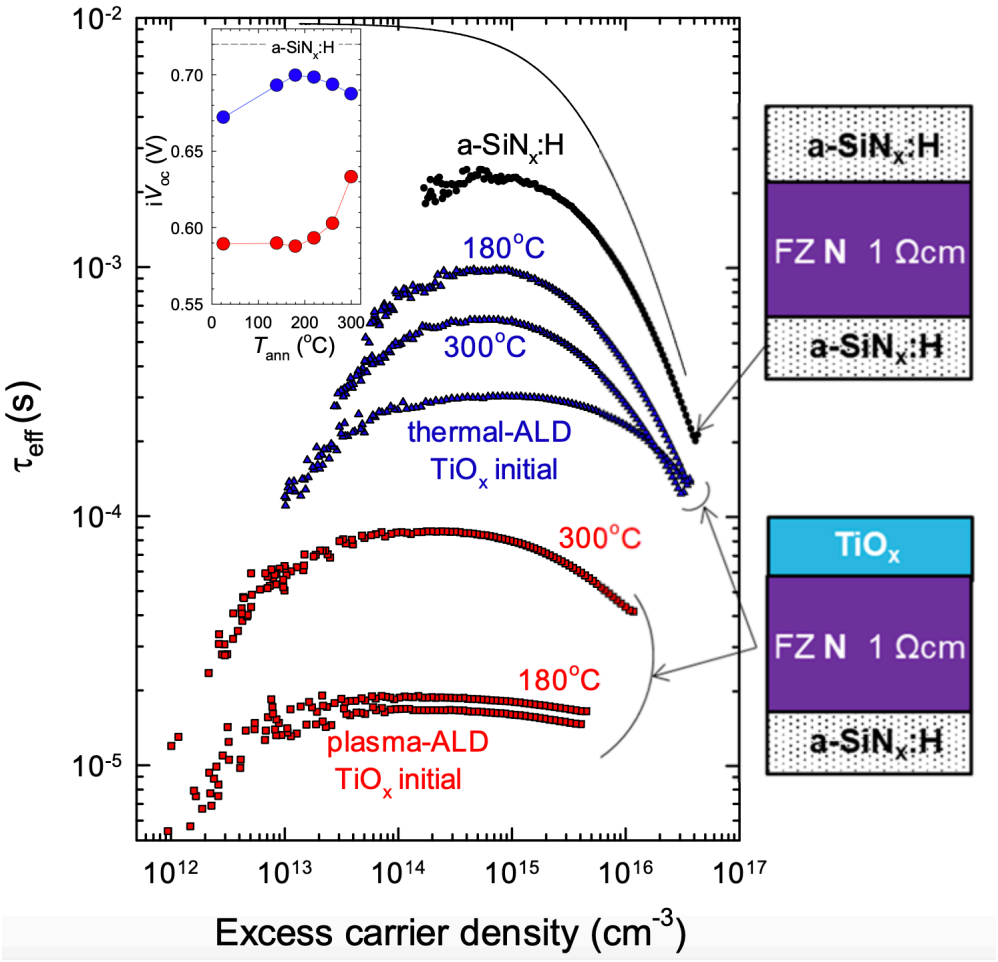

Figure 2. Effective minority carrier lifetime (τ_{eff}) curves as a function of excess carrier density for asymmetrically-passivated TiO_x/(n)c-Si/a-SiN_x:H stack, and symmetrically passivated a-SiN_x:H/(n)c-Si/ a-SiN_x:H as a reference. TiO_x layers were deposited either by plasma- (red) or thermal-ALD (blue). Annealing was repeated at elevated temperatures in the ambient air. The solid line shows the theoretical limit imposed by Auger recombination. Inset shows the iV_{oc} versus annealing temperature (T_{ann}).

Despite of the similar GPC and optical properties, these films exhibit markedly different surface passivation. **Figure 2** shows the carrier-injection-dependent effective lifetime (τ_{eff}) of c-Si wafer measured by QSSPC with an asymmetrically passivated structure: i.e., TiO_x/(*n*)c-Si/a-SiN_x:H, in the initial and annealed states. The TiO_x layer thickness was 6 nm. For comparison, the τ_{eff} curve of a symmetrically a-SiN_x:H passivated samples is also shown. The post-deposition annealing was repeated in ambient air for 15 min at temperatures ranging from T_{ann}=140 to 300 ºC. The reason why we employed the a-SiN_x:H instead of a-Si:H was to maintain passivation quality at relatively high temperatures (~400 ºC). Thus, the measured lifetime in this study reflects the magnitude of carrier recombination at the TiO_x/c-Si interface. It is evident that the passivation quality of the TiO_x markedly differs depending on the ALD process. The thermal-ALD TiO_x shows the higher lifetime in the initial state and it is improved by annealing at 180 ºC. The lifetime reaches 1 ms at an injection level of 10^{15} cm^{-3}, which is nearly the same level of the state-of-the-art ALD-TiO_x reported by other groups,[27] and is only slightly inferior to that of the symmetrically a-SiN_x:H passivated sample. It is noteworthy that such a relatively high passivation quality can be attained when the TiO_x thickness is greater than about ~3 nm. As shown in the inset, the implied V_{oc} (iV_{oc}) at a 1-sun illumination (100 mW cm^{-2}) shows the maximum of 700 mV at an annealing temperature of 180 ºC. Further increasing the annealing temperature results in slight degradation in the lifetime. This tendency is in agreement with the work by Liao *et al*. where they found an optimum annealing temperature at 200-250 ºC.[27] In contrast, the direct deposition of plasma-ALD TiO_x on c-Si results in very poor passivation with lifetime lower than 100 μs, although it is gradually improved by annealing at elevated temperatures. The origin of the different passivation ability of these TiO_x layers is not understood. Yet, it is hypothesized that the incorporated hydrogen from the water vapor in the thermal-ALD TiO_x plays a role in surface passivation. As shown later, an alternative possible explanation is that the fix charge present in the thermal-ALD TiO_x layer provides field-effect passivation.

3.2. Carrier selectivity of TiO_x layers

In general, carrier selectivity reflects how efficiently the internal voltage (the magnitude of the quasi-Fermi level splitting by carrier injection) in the absorber can be extracted to the external circuit.[36] To evaluate this, the difference between iV_{oc} and the external V_{oc} of the solar cells has been investigated.[37] Due to the lack of efficient passivation of some TiO_x-coated samples, it is difficult to conclude whether the solar cell performance is limited by surface recombination or carrier selectivity, if the TiO_x is deposited directly on c-Si. To focus on the carrier selectivity of TiO_x with respect to c-Si absorber, independent of surface passivation, we inserted an intrinsic a-Si:H buffer layer between c-Si and TiO_x. This a-Si:H buffer layer serves as an excellent surface passivation layer, providing an iV_{oc} at 1 sun illumination of above 720 mV regardless of the ALD condition investigated in this study. Hence, it can be assumed that the measured external V_{oc} is governed by the carrier selectivity of TiO_x layer and hence its ability of extracting the iV_{oc} externally.

We fabricated solar cell precursors as shown in **Figure 3**a. By using the appropriate device structure, TiO_x can be evaluated either as electron or hole contact with respect to (*n*) and (*p*)c-Si. In Figure 3b, the corresponding external V_{oc} at a 1-sun illumination measured by suns-V_{oc} are summarized as a figure of merit of the carrier selectivity. In this series, Ti was used as a capping layer on top of the TiO_x, and the results of initial and annealed states are shown. Note that the positive V_{oc} represents the magnitude of electron selectivity (TiO_x and (*n*)a-Si:H as a reference of electron contact) while the negative V_{oc} represents the hole selectivity (TiO_x and (*p*)a-Si:H as a reference of hole contact). It can be seen in Figure 3b that the V_{oc} for the cells with the doped a-Si:H references (white) are very close to their iV_{oc} (~720 mV), as expected for a contact featuring good carrier selectivity.[37] However, the external V_{oc} of solar cell precursors featuring TiO_x contact is typically lower and largely depends on the ALD condition and post annealing. It is clearly indicated that plasma-ALD TiO_x (red) exhibits

better electron selectivity while the thermal-ALD TiO_x (blue) exhibits better hole selectivity instead. This tendency is consistently observed regardless of the doping type of c-Si absorber. Furthermore, the post-deposition annealing is found to decline the electron selectivity whereas it enhances the hole selectivity (except for the samples with thermal-ALD TiO_x used as electron contact). Although the mechanism behind this phenomenon is not well understood, we found that the impact of post-deposition annealing was much greater when annealing the samples after TiO_x/capping layer (Ti, Al, Pd and indium-tin oxide (ITO)) stack compared to annealing before metallization or transparent

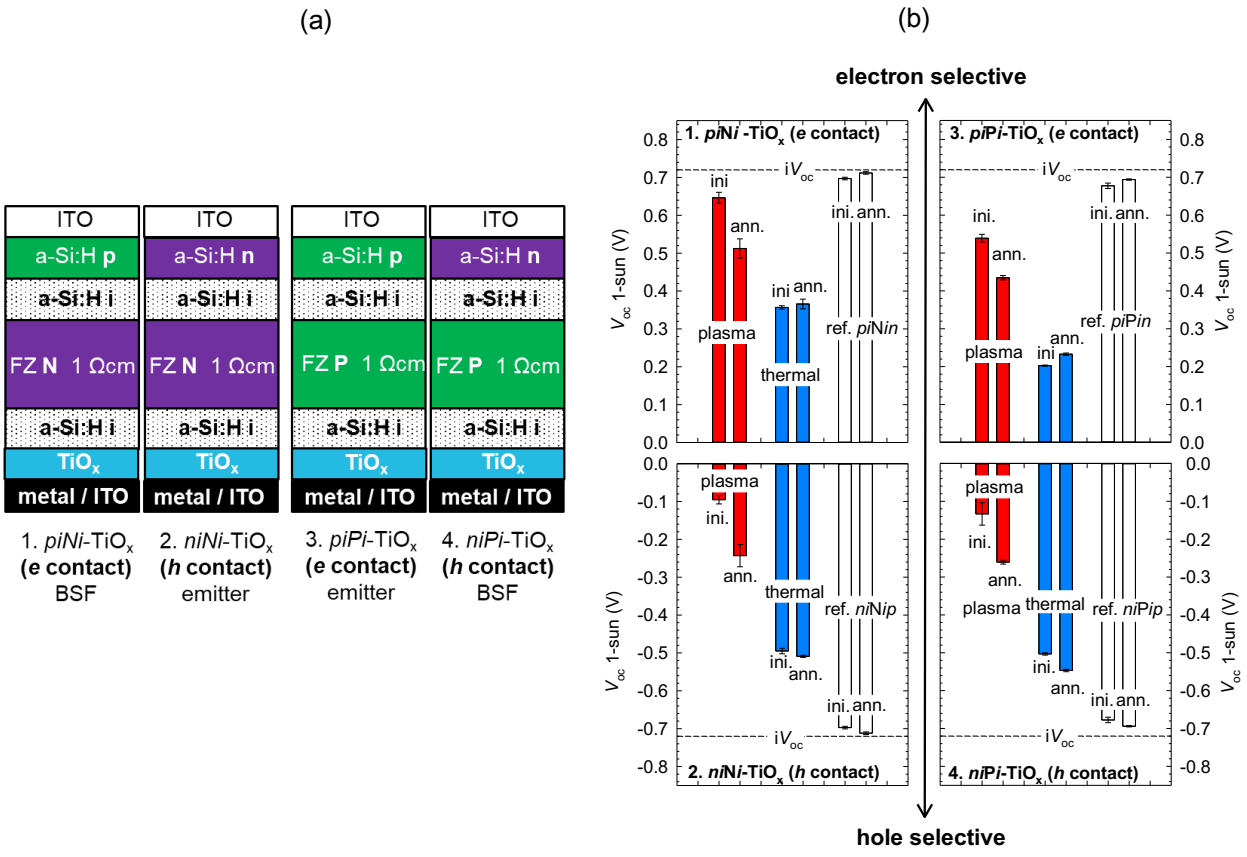

Figure 3. (a) Schematic illustration of sample structures studied in this work. Throughout this study, *n*(*p*) and *N*(*P*) appeared in the figures indicate the carrier type of a-Si:H and c-Si, respectively. (b) Bar charts of external 1-sun V_{oc} in the initial (ini.) and after annealing (ann.) for four different solar cell structures shown in (a). Error bars indicate the spread of multiple measurement data for 1 or 2 samples. A 6-nm-thick TiO_x layer was deposited by either plasma- (red) or thermal-ALD (blue). Ti was used as a capping layer on top of the TiO_x. The results of the standard heterojunction solar cells (white) are also shown for comparison. The dashed lines show the iV_{oc} measured by QSSPC. The positive and negative external V_{oc} represent the magnitude of electron and hole selectivity, respectively.

conductive oxide (TCO) deposition. This suggests that some chemical reaction takes place at the TiO_x/capping layer interface during annealing, influencing the carrier selectivity significantly. According to Yang *et al.*,[17] a chemical reduction reaction of the TiO_x layer is occurred by the covering Al layer during annealing due to the stronger oxygen affinity of Al than Ti. However, they observed improved electron selectivity by post-deposition annealing, which is opposite from our observation. The influence of reducing/oxidizing treatment on the carrier selectivity of TiO_x will be shown later.

3.3. Factors that influence the carrier selectivity

Here we show that carrier selectivity is not governed only by ALD condition of TiO_x layer, but also by other factors. In this section, the results obtained with (*n*)c-Si are shown for simplification. Firstly, it has been revealed that the carrier selectivity and contact resistance of TiO_x are significantly influenced by the capping material.[20-25] **Figure 4** shows the 1-sun external V_{oc} for solar cell precursors plotted versus the work function (WF) of various contact materials (Ti, Al, ITO, Pd).[38,39] The thickness of TiO_x layers was 6 nm. To compare the highest V_{oc} attainable from each solar cell structure, the V_{oc} of initial state are shown for plasma-ALD TiO_x used as electron contact while those of annealed state (180 °C) are shown for thermal-ALD TiO_x used as hole contact. As shown in Figure 4, among four capping materials examined in this study, plasma-ALD TiO_x provides the highest electron selectivity when capped with Al but the lowest one with Pd. A similar result is reported in the solar cells that use $ZnO:SiO_2$ capped with different metals as an electron selective contact.[25] In Figure 4, an almost inverse behavior is observed for the hole selectivity of the thermal-ALD TiO_x. The impact of WF of the capping material on carrier selectivity is much greater when using TiO_x as hole contact (blue, ΔV_{oc}~200 mV) than as electron contact (red, ΔV_{oc}~100 mV) with respect to (*n*)c-Si. By combining TiO_x with the best contact material, almost symmetric carrier selectivity from

electron (V_{oc}~ 680 mV) to hole (V_{oc}~-650 mV) is obtained using the plasma-ALD TiO_x/Al stack and the thermal-ALD TiO_x/ITO stack, respectively. These results indicate that the c-Si band bending is greatly influenced by the WF of the capping material. An exception to this occurs for the thermal-ALD TiO_x/Pd stack, as it shows lower V_{oc} (~580 mV) than that with ITO (~650 mV). Since this TiO_x/Pd stack showed the highest V_{oc} (~630 mV) before annealing (not shown in the figure), it implies that post-deposition annealing of the TiO_x/Pd stack degrades its contact properties. Concerning the effect of annealing, in Figure 4, the V_{oc} of both the initial and annealed states are compared for the case of Al capping layer. The result clearly shows that the impact of the annealing on carrier selectivity is completely opposite between electron and hole contacts, in agreement with the case of Ti capping layer shown in Figure 3b.

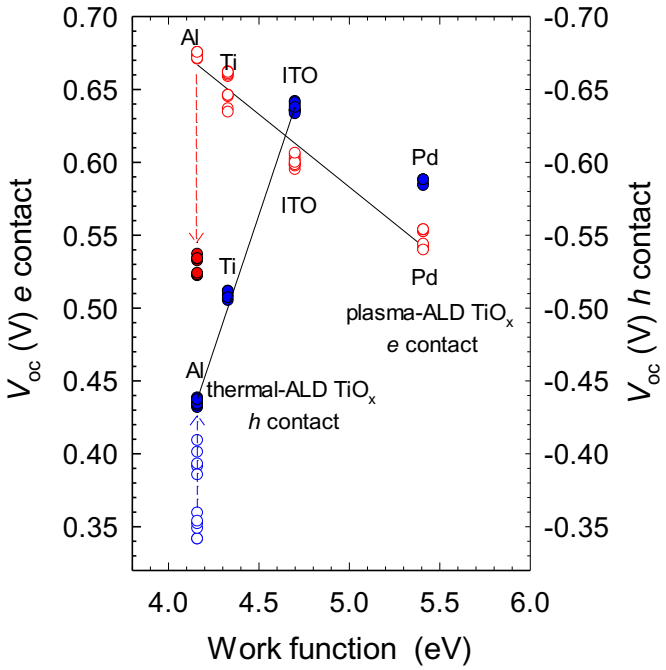

Figure 4. Relationship between the work function of the capping metal or TCO and the external 1-sun V_{oc} of the two solar cell precursors with plasma-ALD TiO_x as electron contact (red) and thermal-ALD TiO_x as hole contact (blue). Open and filled symbols represent the results of the initial and annealed states, respectively.

Secondly, carrier selectivity of TiO_x depends on its thickness, as depicted in **Figure 5**. The TiO_x thickness was varied from 0 to 35 nm for the plasma-ALD TiO_x as electron contact and for the thermal-ALD TiO_x as hole contact. In these plots, the results of the solar cell precursors with the best combination of capping material for the respective contacts (Al for electron contact and ITO for hole contact) are shown. In addition, as previously shown in Figure 4, the V_{oc} of initial state are shown for plasma-ALD TiO_x used as electron contact while those of annealed state are shown for thermal-ALD TiO_x used as hole contact. In Figure 5, the V_{oc} of both solar cells increase abruptly from the very low values less than 400 mV to more than 650 mV by depositing only a few nanometer-thick TiO_x layers. This clearly shows that the external V_{oc} cannot be extracted efficiently without applying any carrier selective contact. It is worth emphasizing that the highest V_{oc} of 720 mV, which is closed to the maximum attainable values (iV_{oc}), is obtained for the plasma-ALD TiO_x used as an electron contact with a thickness of 3 nm. Thus, it is demonstrated that the plasma-ALD TiO_x can work as an efficient electron contact comparable to the (*n*)a-Si:H. Unlike the doped a-Si:H,[40] however, V_{oc} decreases gradually with

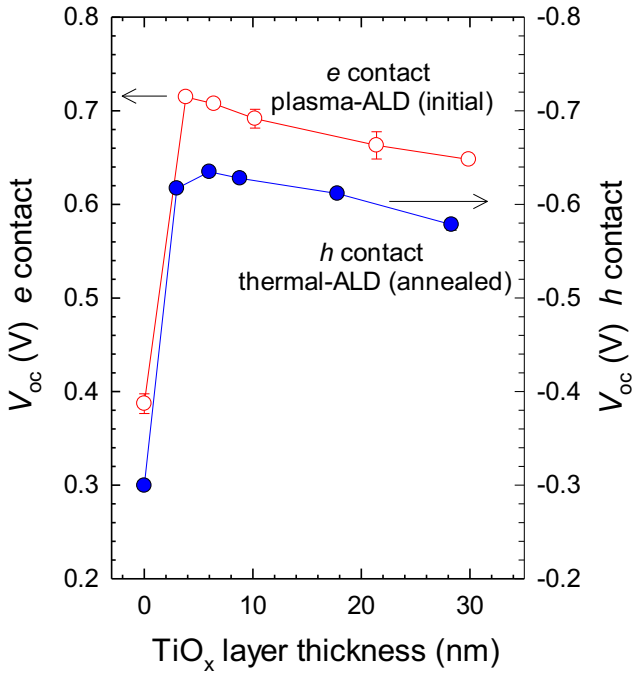

Figure 5. External 1-sun V_{oc} as a function of TiO_x thickness. Plasma-ALD TiO_x/Al (red) and thermal-ALD TiO_x/ITO (blue) stacks were used for electron and hole contacts, respectively. Open and filled symbols represent the results of the initial and annealed states, respectively.

increasing thickness of the TiO_x layer for both solar cell structures. This implies that, as the TiO_x becomes thinner, a stronger electric field is created in the TiO_x layer by the contact with either low or high WF material presumably due to the low carrier density in TiO_x. Such an internal electric field in TiO_x might play a role in the carrier extraction from c-Si to electrode through the TiO_x layer.

Finally, we show the impact of reducing/oxidizing treatment on the carrier selectivity of TiO_x. **Figure 6** shows the 1-sun external V_{oc} of solar cell precursors with various plasma treatments applied to the 6-nm-thick TiO_x surface. Plasma treatments with three different gases of H_2, O_2 and Ar were examined in the same ALD chamber using a remote ICP source. Each

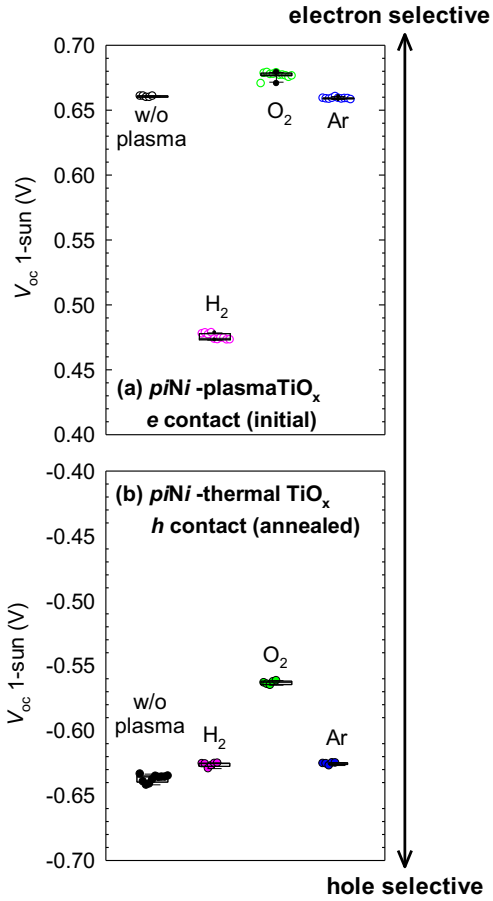

Figure 6. Impact of various plasma treatments (H_2, O_2 and Ar) of TiO_x layers on 1-sun external V_{oc} of the two solar cell precursors with (a) plasma-ALD TiO_x/Al as electron contact and (b) thermal-ALD TiO_x/ITO as hole contact. The positive and negative external V_{oc} represent the magnitude of electron and hole selectivity, respectively. Open and filled symbols represent the results of the initial and annealed states, respectively.

plasma treatment was done for 15 min at 200 ºC under the same pressure and rf power used for plasma-ALD process. We confirmed that the thickness of TiO_x layer and the surface passivation remain unchanged after these plasma treatments. In Figure 6a, a massive decrease of electron selectivity (ΔV_{oc}~200 mV) was observed when exposing plasma-ALD TiO_x to H_2 plasma treatment. In contrast, oxygen plasma treatment provides a slight enhancement of electron selectivity. On the other hand, for thermal-ALD TiO_x used as a hole contact shown in Figure 6b, H_2 plasma treatment does not change much the carrier selectivity while the O_2 plasma decreases the hole selectivity (ΔV_{oc}~80 mV). Since no notable change in carrier selectivity was observed when exposing these TiO_x layers to inert Ar gas plasma, we conclude that the change in carrier selectivity after H_2 or O_2 plasma treatment is attributed to the chemical reaction of TiO_x rather than the ion bombardment or UV radiation. These results support the idea that the redox reaction (chemical composition) of TiO_x layer is crucial in determining the carrier selectivity.

3.4. SPV and C-V measurements

To gain more insight into the origin of the carrier selectivity of TiO_x, we measured SPV for the 6-nm-thick plasma- and thermal-ALD TiO_x deposited on (*n*) and (*p*)c-Si without a-Si:H buffer layer. **Figure 7** shows the induced c-Si band bending (Φ) measured by SPV before and after annealing at 180 ºC in the ambient air. For comparison, the measured Φ for (*n*) and (*p*)a-Si:H layers (~10 nm) deposited on the same substrates are included. These doped a-Si:H contacts demonstrate an ideal band bending (>800 mV) when deposited on the c-Si that has an opposite polarity. It is evident that plasma- and thermal-ALD TiO_x induce the band bending in an opposite way, i.e., plasma-ALD TiO_x induces slightly larger or similar band bending for (*p*)c-Si than for (*n*)c-Si while the thermal-ALD TiO_x induces strong band bending (>800 mV) only for (*n*)c-Si. It should be added that an insertion of the a-Si:H buffer layer between TiO_x

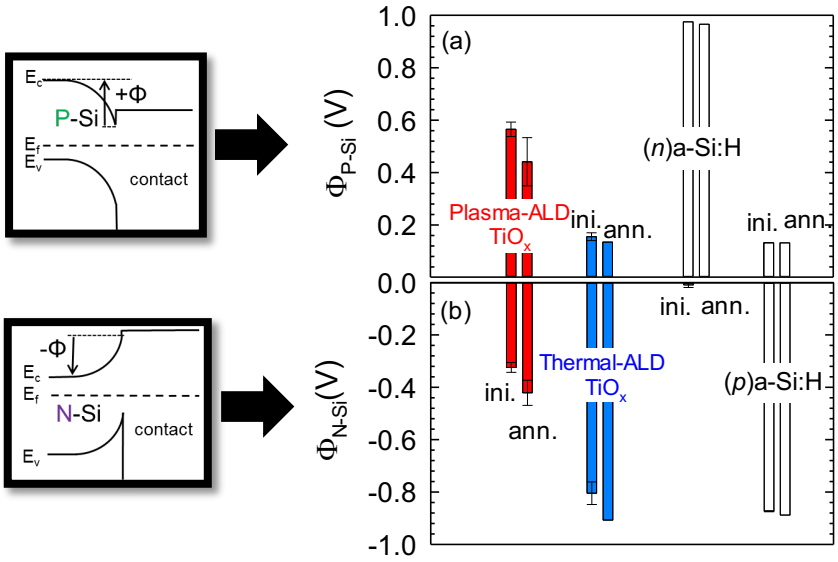

Figure 7. SPV signals (Φ) measured for TiO_x layers deposited on (a) *p*- and (b) *n*-type c-Si in the initial (ini.) and annealed (ann.) states. Error bars indicate the spread of multiple measurement data for 1 or 2 samples. TiO_x was deposited by plasma- (red) or thermal-ALD (blue). For comparison, SPV signals for a-Si:H *n* and *p* layers are also shown.

and c-Si, which was used for the solar cell precursors in this study, did not alter the observed tendency, while it tends to increase SPV signal for (*p*)c-Si and decrease it for (*n*)c-Si by ~200 mV. This indicates that the undoped a-Si:H behaves as a weak electron selective contact.

To clarify the origin of the induced band bending by TiO_x layers, we performed C-V measurements on a GaIn/(*n*)c-Si/TiO_x/Al MIS structures. **Figure 8** shows the measured C-V curves at various frequencies for the ~6-nm-thick plasma- and thermal-ALD TiO_x without annealing, including simulated C-V curves in order to infer the characteristics of the TiO_x layers. As reported by other authors,[27,41] TiO_x films are extremely leaky and thus parameters from the C-V measurements are difficult to be extracted quantitatively. Nevertheless, comparison of the data in Figure 8 to simulated C-V curves can elucidate the properties of the c-Si/TiO_x interface. In Figure 8, the typical behavior of leaky insulators is evidenced by the increase in the oxide capacitance, normally measured when the semiconductor is in accumulation regime $-V_{bias} >> 0$, as the measurement frequency decreases.[33] Leakage is also evidenced in the strong dip observed in the capacitance in this regime. Characterizing the charge of the dielectrics requires the calculation of the flat-band voltage in these devices, which cannot be found without accurate

knowledge of the oxide capacitance. To overcome this, simulations of the high frequency capacitance have been carried out using typical device parameters, and following the formulation outlined by Sze.[42] Here, it is clear that the shift in flat-band voltage (ΔV) is substantially different for samples with plasma- versus thermal-ALD TiO_x. In plasma-ALD TiO_x, a shift of -0.44 V can be partially explained by the WF difference between the top aluminum contact (Φ_m~4 eV) and that of 1 Ωcm (*n*)c-Si (Φ_m~4.27 eV), contributing ~ 0.27 V shift, and possibly by a concentration of charged interface states (Q_{it}) in the flat-band condition, as remarked in references.[42-44] For thermal-ALD TiO_x, on the other hand, a shift of +0.55 V cannot be explained by Q_{it}, since it would require an excessively large concentration of negatively charged interface acceptor states, which would increase surface recombination, and it is thus in disagreement with the high lifetime results in Section 3.1. Here it is concluded that up to 0.82 V of shift is produced due to negative charge inside the TiO_x film, when accounting for the WF difference. If all this charge is assumed to be at the TiO_x–Si interface, and the insulator capacitance is >1 μF cm^{-2}, a charge concentration of at least 5×10^{12} cm^{-2} is inferred to be present in the TiO_x film.

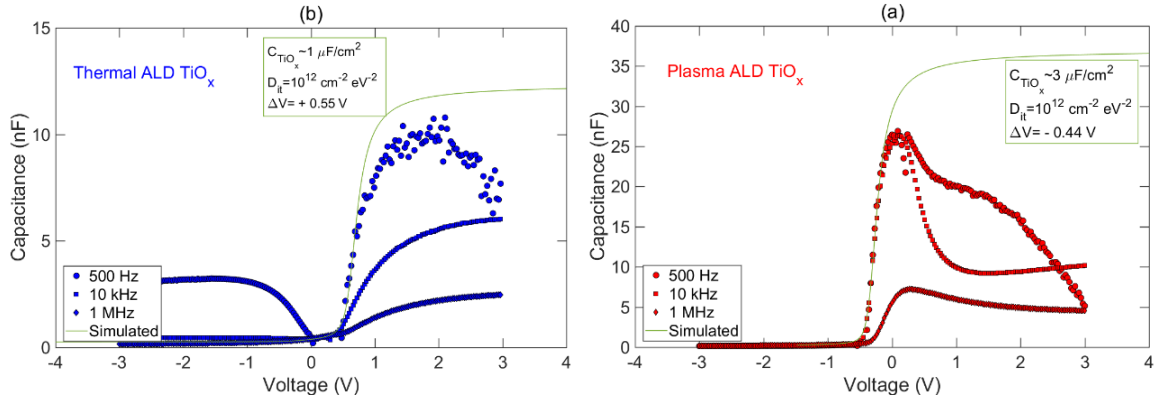

Figure 8. C-V measurements of GaIn/(*n*)c-Si/TiO_x/Al MIS structures for (a) plasma- and (b) thermal-ALD TiO_x, including simulated C-V curves to infer the concentration of charge in the TiO_x films from their flat-band shift. Samples were not annealed.

4. Discussion

4.1. Origin of the carrier selectivity

Our results revealed that TiO_x can act as either electron or hole selective contact depending on ALD process, and its selectivity is strongly influenced by many factors including thickness of the TiO_x layer, post-deposition annealing, post plasma-treatment, and WF of metal or TCO contact on top of TiO_x layer. In particular, we found that the TiO_x can be tuned to work as a hole contact in c-Si solar cells. This is associated with the fact that the deposition of thermal-ALD TiO_x on (*n*)c-Si provides a large band bending of 900 mV. We confirmed that the band bending of ~900 mV is comparable to the case when Al_2O_3 layers are deposited on (*n*)c-Si by ALD. The creation of such band bending by the deposition of the dielectric layer is known to originate from the negative fixed charge present at the Si/Al_2O_3 interface with a density of ~ 10^{13} q cm^{-2}.[45] Our C-V measurement on the TiO_x layers suggests that the similar amount of the negative charge is present at the Si/TiO_x interface, although the accurate quantification is difficult due to the semiconducting behavior of TiO_x layer. The presence of the negative charge in TiO_x has been predicted, and the use of TiO_x as a field-effect passivation layer for the heavily boron-doped silicon is proposed to repel the minority carriers (electrons).[28,35]

As shown in **Figure 9**, we found a good correlation between external V_{oc} of solar cell precursors (shown in Figure 3b) versus induced c-Si band bending measured by SPV (shown in Figure 7). Note that the horizontal axis in Figure 9 represents the band bending (inversion) induced in the c-Si that has the asymmetric polarity (i.e., (*p*) and (*n*)c-Si were used in the SPV measurement for the evaluation of the induced-band bending created by electron and hole contacts, respectively). Regardless of the (*n*) or (*p*)c-Si absorber, the V_{oc} of solar cells shown in Figure 9 are well fitted by the linear regression as a function of the amount of band bending. This suggests that the asymmetric induced-band bending in c-Si is an effective measure to

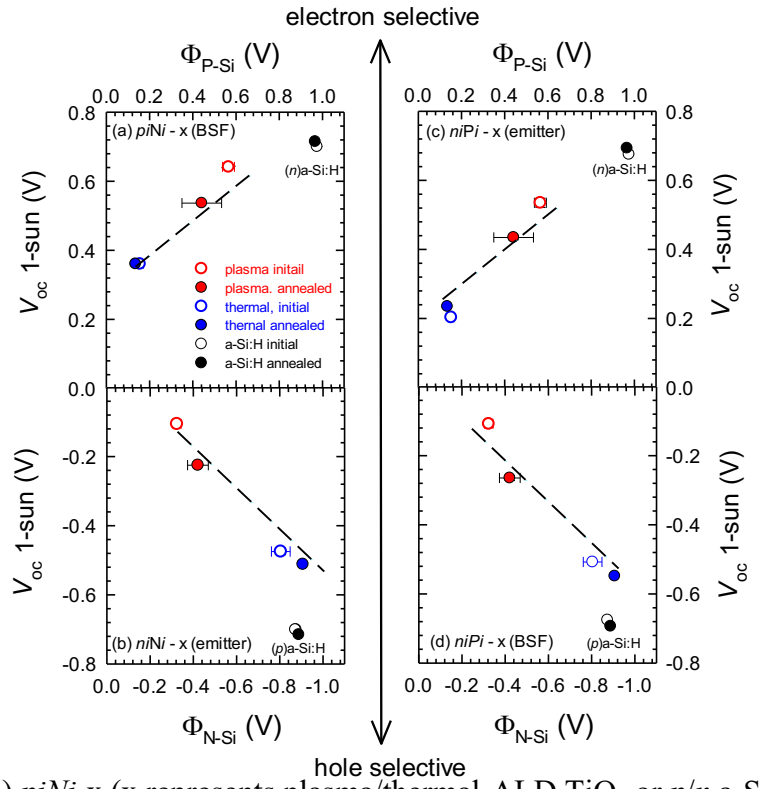

Figure 9. V_{oc} of (a) *piNi*-x (x represents plasma/thermal-ALD TiO_x or *p*/*n* a-Si:H) and (b) *niNi*-x samples taken from the data in Figure 3b, plotted versus Φ measured on *P*/x and *N*/x contacts taken from the data in Figure 7, respectively. Similarly, the data are plotted for (*p*)c-Si base in (c) and (d). Open and closed symbols represent the initial and annealed states, respectively.

evaluate the magnitude of carrier selectivity.[44] Nevertheless, this linear regression does not follow when including the results of the standard SHJ solar cells, particularly for the hole contact. This originates from the fact that the carrier selectivity of TiO_x strongly depends on the capping layer, and unoptimized metal (Ti) was chosen in this series. Doping in a-Si:H is known to change its WF while it does not create fixed charge in the material. Therefore, it suggests that the control of WF might be more effective than creating the fixed charge in the contact in terms of carrier selectivity.

In **Figure 10**, possible band diagrams of the (*n*)c-Si/(*i*)a-Si:H/TiO_x/capping layer stacks are shown. As previously shown in Figure 5, the solar cell provides very low V_{oc} (300-400 mV) unless the carrier selective contact such as TiO_x and doped a-Si:H is applied at the Si/metal (TCO) contact. This has been explained by the Fermi-level pinning at the Si/metal contact. As

shown in Figure 10 (a), once the plasma-ALD TiO_x is incorporated, an ideal electron contact is formed due to the Fermi-level depinning.[21] However, the large band bending with an opposite polarity is created when deposited the thermal-ALD because of the presence of the negative fixed charge (Figure 10 (b)). This induced band bending can be maintained when the high WF metal or TCO was deposited on top of TiO_x layer. From our results, the classical understanding of the carrier selectivity based on the band offset at the Si/metal-oxide contact does not fully account for the observed carrier selectivity because our thermal-ALD TiO_x acts as hole selective contact despite of the presumed presence of the large valence band offset at the Si/TiO_x interface. This suggests that the valence band offset does not act as a perfect hole blocking, allowing the hole extraction to the external circuit. Although the carrier transport at the Si/TiO_x interface is not clarified yet, the minority holes are considered to be collected at the electrode probably by the recombination with electron at the Si/TiO_x contact and/or the efficient trap-assisted tunneling path in TiO_x.[47,48]

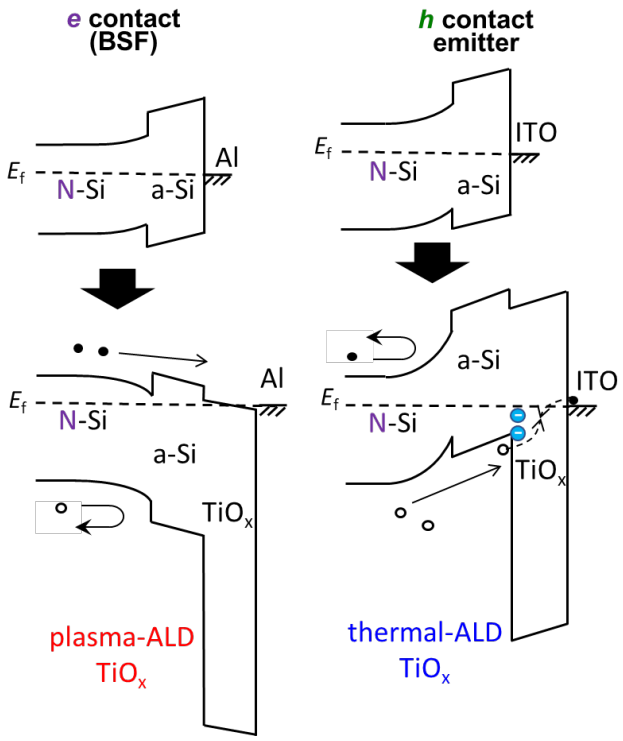

Figure 10. Possible band diagrams of the c-Si/(*i*)a-Si:H/TiO_x contact system explaining the inverse carrier selective behaviors observed in the (a) plasma- and (b) thermal-ALD TiO_x. To highlight the role of the TiO_x layer, the contact systems with direct metal (TCO) contact are shown.

4.2. Comparison to preceding works

Yang *et al*. has demonstrated that TiO_x thin layer grown by thermal-ALD performs good electron contact for (*n*)c-Si.[20] They showed the relatively high V_{oc} of solar cell using a full-area TiO_x/Al rear contact and a boron-diffused front emitter. A very thin SiO_2 buffer layer was introduced at the Si/TiO_x interface to improve the surface passivation, leading to a V_{oc} of 674 mV and an efficiency of 22.1%. Although our plasma-ALD TiO_x with an (*i*)a-Si:H buffer layer shows relatively good electron selectivity (V_{oc}~720 mV), the thermal-ALD TiO_x shows the completely inverse behavior with respect to their work. This might be an unusual result, being attributed to the presence of a number of fixed negative charge in the TiO_x. In fact, in our best knowledge, TiO_x as hole contact has not been reported so far in solar cell application. Nevertheless, the thermal-ALD TiO_x layers have shown to work as hole transport layers as well as corrosion resistive layers in photocatalysis for water splitting application.[49,50] We believe that these TiO_x layers function in a similar way to our thermal-ALD TiO_x. Furthermore, it is plausible that the hole selectivity of these TiO_x is enhanced by the formation of the high WF metal catalysts such as Ir [49] and Ni [50] on top of the TiO_x layer.

The negative charge in TiO_x has been attributed to the oxygen vacancies in TiO_x which can be neutralized by annealing in oxygen ambient.[26] From our post-deposition oxygen plasma treatments, we found that the plasma oxidation of the TiO_x leads to lower hole selectivity. These are qualitatively in good agreement. Thus, it is plausible that the thermal-ALD TiO_x contains a number of oxygen vacancies probably due to the low reactivity between TTIP and H_2O. The presence of hydrogen in the thermal-ALD process is also a possible source of creating oxygen vacancies in TiO_x.

We have seen a good agreement with the work by Yang *et al*. in terms of the influence of the WF of metal (TCO) layer that covers the TiO_x. Among the materials investigated, Al was the best choice for electron contact because of its low WF. Similarly, Allen *et al*. reported that the deposition of Ca as a very low WF metal (<3 eV) on ALD-TiO_x led to an improved electron

contact in comparison with the case of Al.[22] Recently, Cho *et al*. reported that the thermal-ALD TiO_x from the same precursor (TTIP) demonstrates good electron contact (V_{oc}~700 mV) by using Ca as a capping layer.[19] Based on these results, it is likely that the carrier density in TiO_x is too low so that the screening length of the TiO_x layer is greater than its thickness. We highlight that the need for a capping layer featuring a low WF is a notable disadvantage because it limits the applicability of TiO_x in practical contact systems, as high efficiency device requires not only good electrical contact but also proper optical design that often includes low-refractive-index TCO layer to enhance the optical reflection at the rear contact. In this regard, the use of TiO_x/TCO stack as a hole selective contact will be an interesting subject of research, as it provides an ideal optical transmission and reflection at the front and rear contacts, respectively.

5. Conclusions

We have studied interface electrical properties of TiO_x nanolayers deposited by ALD for their application as carrier selective contacts in (*n*) and (*p*)c-Si. Two different oxidation processes in ALD, i.e., plasma- and thermal-ALD, have been employed, which results in a similar film growth rate per cycle and similar optical constants, but markedly different c-Si surface passivation capability. To focus on the carrier selectivity of TiO_x independent from the surface passivation, we have used an (*i*)a-Si:H buffer layer to maintain the good surface passivation regardless of the ALD condition. We measured V_{oc} as a figure of merit of its carrier selectivity for specially designed solar cell precursors, using TiO_x as either electron or hole contact. While TiO_x has been traditionally considered to act as an electron selective contact in c-Si solar cell, we find that TiO_x can act as a hole selective contact as well, depending on the oxidation process in the ALD. We also show that carrier selectivity of TiO_x is strongly influenced by various factors including the post-deposition annealing, plasma treatment, the WF of the capping layer, and TiO_x thickness. As a result, it is demonstrated that the carrier

selectivity of TiO_x can be widely tunable from electron (V_{oc}~680-720 mV) to hole selectivity (V_{oc}~650 mV). This completely inverse behavior in terms of carrier selectivity using the same material is qualitatively correlated with the polarity and the amount of the band bending induced in c-Si by TiO_x layer. This is further supported by the C-V measurements, from which a large amount of fixed negative charge (at least 5×10^{12} cm^{-2}) is inferred to be present in the thermal-ALD TiO_x layer. Our results revealed that the carrier selectivity is governed by the asymmetric band bending in c-Si induced by the difference of effective work function as well as by fixed charge in the TiO_x. This gives a qualitative explanation for the observed carrier selectivity, and it is in contrast to the previous understanding that the carrier selectivity is determined by the asymmetric band offset at the c-Si/TiO_x interface alone. Further study is necessary to elucidate the hole transport mechanism through the energy barrier at the c-Si/TiO_x interface.

The implementation of the TiO_x contact without a-Si:H buffer layer is of practical importance for the actual solar cell application, which will be reported in a follow up study. In particular, the application of TiO_x as a hole selective passivating contact is an interesting novel approach, as it provides both good surface passivation and hole selectivity.

Acknowledgements

The authors are grateful to A. Richter and F. Feldmann for valuable discussions, and K. Zimmermann, A. Leimenstoll, F. Schätzle, N. Braendlin, F. Zähringer, H. Steidl, C. Schetter for technical assistance with deposition setups and sample processing. T. Matsui acknowledges the other co-workers at Fraunhofer ISE for their help, and financial support from AIST for international research exchange program.

Part of this work has received funding from the European Union's Horizon 2020 Research and Innovation programme under grant agreement No 727529 Project DISC. R. S. Bonilla is recipient of a Royal Academy of Engineering Research Fellowship, UK, and acknowledges the support from ESPRC Postdoctoral Fellowship EP/M022196/1.

References

[1] U. Würfel, A. Cuevas, P. Würfel, Charge carrier separation in solar cells, *IEEE J. Photovoltaics*. **5** (2015) 461-469.

[2] K. Masuko, M. Shigematsu, T. Hashiguchi, D. Fujishima, M. Kai, N. Yoshimura, T. Yamaguchi, Y. Ichihashi, T. Mishima, N. Matsubara, T. Yamanishi, T. Takahama, M. Taguchi, E. Maruyama, S. Okamoto, Achievement of more than 25% conversion efficiency with crystalline silicon heterojunction solar cell, *IEEE J. Photovoltaic*s. **4** (2014) 1433-1435.

[3] K. Yoshikawa, H. Kawasaki, W. Yoshida, T. Irie, K. Konishi, K. Nakano, T. Uto, D. Adachi, M. Kanematsu, H. Uzu, K. Yamamoto, Silicon heterojunction solar cell with interdigitated back contacts for a photoconversion efficiency over 26%, *Nat. Energy*. **2** (2017) 17032.

[4] F. Feldmann, M. Bivour, C. Reichel, M. Hermle, S.W. Glunz, Passivated rear contacts for high-efficiency n-type Si solar cells providing high interface passivation quality and excellent transport characteristics, *Sol. Energy Mater. Sol. Cells.* **120** (2014) 270-274.

[5] A. Richter, J. Benick, F. Feldmann, A. Fell, M. Hermle, S.W. Glunz, n-Type Si solar cells with passivating electron contact: Identifying sources for efficiency limitations by wafer thickness and resistivity variation, *Sol. Energy Mater. Sol. Cells*. **173** (2017) 96-105.

[6] F. Haase, C. Hollemann, S. Schäfer, A. Merkle, M. Rienäcker, J. Krügener, R. Brendel, R. Peibst, Laser contact openings for local poly-Si-metal contacts enabling 26.1%-efficient POLO-IBC solar cells, *Sol. Energy Mater. Sol. Cells.* **186** (2018) 184-193.

[7] C. Battaglia, X. Yin, M. Zheng, ID. Sharp, T. Chen, S. McDonnell, A. Azcatl, C. Carraro, B. Ma, R. Maboudian, R.M. Wallace, A. Javey, Hole selective MoO_x contact for silicon solar cells, *Nano Lett*. **14** (2014) 967-971.

[8] M. Bivour, J. Temmler, H. Steinkemper, M. Hermle, Molybdenum and tungsten oxide: High work function wide band gap contact materials for hole selective contacts of silicon solar cells, *Sol. Energy Mater. Sol. Cells*. **142** (2015) 34-41.

[9] L.G. Gerling, S. Mahato, A. Morales-Vilches, G. Masmitja, P. Ortega, C. Voz, R. Alcubilla, J. Puigdollers, Transition metal oxides as hole-selective contacts in silicon heterojunctions solar cells, *Sol. Energy Mater. Sol. Cells*. **145** (2016) 109-115.

[10] H.S. Kim, J.E. Park, M. Patel, H. Kim, D.S. Kim, S.K. Byeon, D. Lim, J. Kim, Optically transparent and electrically conductive NiO window layer for Si solar cells, *Materials Letters*. **174** (2016) 10-13.

[11] Y. Wan, C. Samundsett, J. Bullock, T. Allen, M. Hettick, D. Yan, P. Zheng, X. Zhang, J. Cui, J. McKeon, A. Javey, A. Cuevas, Magnesium fluoride electron-selective contacts for crystalline silicon solar cells, *ACS Appl. Mater. Interfaces*. **8** (2016) 14671-14677.

[12] Y. Wan, C. Samundsett, J. Bullock, M. Hettick, T. Allen, D. Yan, J. Peng, Y. Wu, J. Cui, A. Javey, A. Cuevas, Conductive and stable magnesium oxide electron-selective contacts for efficient silicon solar cells, *Adv. Energy Mater*. **7** (2017) 1601863.

[13] Y.F. Zhang, R.Y. Liu, S.T. Lee, B.Q. Sun, The role of a LiF layer on the performance of poly(3,4-ethylenedioxythiophene):poly(styrenesulfonate)/Si organic-inorganic hybrid solar cells, *Appl. Phys. Lett*. **104** (2014) 083514.

[14] S. Avasthi, W.E. McClain, G. Man, A. Kahn, J. Schwartz, J.C. Sturm, Hole-blocking titanium-oxide/silicon heterojunction and its application to photovoltaics, *Appl. Phys. Lett.* **102** (2013) 203901.

[15] K.A. Nagamatsu, S. Avasthi, G. Sahasrabudhe, G. Man, J. Jhaveri, A.H. Berg, J. Schwartz, A. Kahn, S. Wagner, J.C. Sturm, Titanium dioxide/silicon hole-blocking selective contact to enable double-heterojunction crystalline silicon-based solar cell, *Appl. Phys. Lett*. **106** (2015) 123906.

[16] X. Yang, P. Zheng, Q. Bi, K. Weber, Silicon heterojunction solar cells with electron selective TiOx contact, *Sol. Energy Mater. Sol. Cells.* **150** (2016) 32-38.

[17] X. Yang, Q. Bi, H. Ali, K. Davis, W.V. Schoenfeld, K. Weber, High-performance TiO_2-based electron-selective contacts for crystalline silicon solar cells, *Adv. Mater*. **28** (2016) 5891.

[18] J. Bullock, Y. Wan, Z. Xu, S. Essig, M. Hettick, H. Wang, W. Ji, M. Boccard, A. Cuevas, C. Ballif, A. Javey, Stable dopant-free asymmetric heterocontact silicon solar cells with efficiencies above 20%, *ACS Energy Lett.* **3** (2018) 508-513.

[19] J. Cho, J. Melskens, M. Debucquoy, M. Recamán Payo, S. Jambaldinni, T. Bearda, I. Gordon, J. Szlufcik, W.M.M. Kessels, J. Poortmans, Passivating electron-selective contacts for silicon solar cells based on an a-Si:H/TiO_x stack and a low work function metal, *Prog. Photovolt. Res. Appl.* **26** (2018) 835-845.

[20] X. Yang, K. Weber, Z. Hameiri, S. De Wolf, Industrially feasible, dopant-free, carrier-selective contacts for high-efficiency silicon solar cells, *Prog. Photovolt. Res. Appl.* **25** (2017) 896-904.

[21] A. Agrawal, J. Lin, M. Barth, R. White, B. Zheng, S. Chopra, S. Gupta, K. Wang, J. Gelatos, S.E. Mohney. S. Datta, Fermi level depinning and contact resistivity reduction using a reduced titania interlayer in n-silicon metal-insulator-semiconductor ohmic contacts, *Appl. Phys. Lett*. **104** (2014) 112101.

[22] T.G. Allen, J. Bullock, Q. Jeangros, C. Samundsett, Y. Wan, J. Cui, A. Hessler-Wyser, S. De Wolf, A. Javey, A. Cuevas, A low resistance calcium/reduced titania passivated contact for high efficiency crystalline silicon solar cells, *Adv. Energy Mater.* **7** (2017) 1602606.

[23] T. Matsui, M. Bivour, P. Ndione, P. Hettich, M. Hermle, Investigation of atomic-layer-deposited TiO_x as selective electron and hole contacts to crystalline silicon, *Energy Procedia*. **124** (2017) 628-634.

[24] T.G. Allen, J. Bullock, X. Yang, A. Javey, S. De Wolf, Passivating contacts for crystalline silicon solar cells, *Nature Energy*, **4** (2019) 914–928.

[25] S. Zhong, M. Morales-Masis, M. Mewsd, L. Korted, Q. Jeangrosa, W. Wua, M. Boccard, C. Ballif, Exploring co-sputtering of ZnO:Al and SiO_2 for efficient electron-selective contacts on silicon solar cells, *Sol. Energy Mater. Sol. Cells*, **194** (2019) 67-73[26]

[26] K.R. McIntosh, S.C. Baker-Finch, N.E. Grant, A.F. Thomson, S. Singh, I.D. Baikie, Charge density in atmospheric pressure chemical vapor deposition TiO_2 on SiO_2-passivated silicon, *J. Electrochem. Soc*. **156** (2009) G190-G195.

[27] B. Liao, B. Hoex, A.G. Aberle, D. Chi, C.S. Bhatia, Excellent c-Si surface passivation by low-temperature atomic layer deposited titanium oxide, *Appl. Phys. Lett*. **104** (2014) 253903.

[28] J. Cui, T. Allen, Y. Wan, J. Mckeon, C. Samundsett, D. Yana, X. Zhang, Y. Cui, Y. Chen, P. Verlinden, A. Cuevas, Titanium oxide: A re-emerging optical and passivating material for silicon solar cells, *Sol. Energy Mater. Sol. Cells*. **158** (2016) 115-121.

[29] R.A. Sinton, A. Cuevas, in *16th Eur. Photovoltaic Solar Energy Conf.*, WIP Munich, (2000) pp. 1152-1155.

[30] R.A. Sinton, A. Cuevas, Contactless determination of current-voltage characteristics and minority-carrier lifetimes in semiconductors from quasi-steady-state photoconductance data, *Appl. Phys. Lett*. **69** (1996) 2510.

[31] K. Heilig, Determination of surface properties by means of large signal photovoltage pulses and the influence of trapping, *Surf. Sci.* **44** (1974) 421.

[32] C. Leendertz, N. Mingirulli, T.F. Schulze, J.P. Kleider, B. Rech, L. Korte, Discerning passivation mechanisms at a-Si:H/c-Si interfaces by means of photoconductance measurements, *Appl. Phys. Lett*. **98** (2011) 202108.

[33] E.H. Nicollian, J.R. Brews, *MOS (Metal Oxide Semiconductor) — Physics and Technology*. Wiley, New York, (1982).

[34] M. Ritala, M. Leskelä, L. Niinistö, P. Haussalo, Titanium isopropoxide as a precursor in atomic layer epitaxy of titanium dioxide thin films, *Chem. Mater.* **5** (1993) 1174-1181.

[35] B. Liao, B. Hoex, K.D. Shetty, P.K. Basu, C.S. Bhatia, Passivation of boron-doped industrial silicon emitters by thermal atomic layer deposited titanium oxide, *IEEE J. Photovolt.* **5** (2015) 1062-1066.

[36] S.W. Glunz, M. Bivour, C. Messmer, F. Feldmann, R. Müller, C. Reichel, A. Richter, F. Schindler, J. Benick, M. Hermle, in *44th IEEE Photovoltaics Specialist Conf.*, IEEE, Piscataway, NJ, USA, (2017) pp. 2064-2069.

[37] M. Bivour, M. Reusch, S. Schroer, F. Feldmann, J. Temmler, H. Steinkemper, M. Hermle, Doped layer optimization for silicon heterojunctions by injection-level-dependent open-circuit voltage measurements, *IEEE J. Photovoltaics*. **4** (2014) 566-574.

[38] W.M. Haynes, *CRC Handbook of Chemistry and Physics, 92nd ed.,* CRC Press, Boca Raton, FL, USA, (2012).

[39] A. Klein, C. Körber, A. Wachau, F. Säuberlich, Y. Gassenbauer, R. Schafranek, S.P. Harvey, T.O. Mason, Surface potentials of magnetron sputtered transparent conducting oxides, *Thin Solid Films*. **518** (2009) 1197-1207.

[40] H. Fujiwara, M. Kondo, Effects of a-Si:H layer thicknesses on the performance of a‐Si:H/c-Si heterojunction solar cells, *J. Appl. Phys.* **101** (2007) 054516.

[41] R.S. Bonilla, K.O. Davis, E.J. Schneller, W.V. Schoenfeld, P.R. Wilshaw. Effective antireflection and surface passivation of silicon using a SiO_2/a-TiO_x film stack, *IEEE J. Photovolt.* **7** (2017) 1603-1610.

[42] S.M. Sze, K.K. Ng, *Physics of Semiconductor Devices*, *3rd ed*., John Wiley and Sons, Inc, Hoboken, NJ, USA, (2007).

[43] D.K. Schroder, *Semiconductor Material and Device Characterization*, John Wiley & Sons, Inc., Hoboken, NJ, USA, (2006).

[44] R.S. Bonilla, N. Jennison, D. Clayton-Warwick, K.A. Collett, L. Rands, P.R. Wilshaw, Corona charge in SiO_2: Kinetics and surface passivation for high efficiency silicon solar cells, *Energy Procedia.* **92** (2016) 326.

[45] B. Hoex, J. Schmidt, P. Pohl, M.C.M. van de Sanden, W.M.M. Kessels, Silicon surface passivation by atomic layer deposited Al_2O_3, *J. Appl. Phys.* **104** (2008) 044903.

[46] M. Bivour, C. Messmer, L. Neusel, F. Zähringer, J. Schön, S.W. Glunz, M. Hermle, in *33rd Eur. Photovoltaic Solar Energy Conf. and Exhibition*, WIP Munich, (2017) pp. 348‑352.

[47] Y. Liu, P. Stradins, H. Deng, J. Luo, S-H. Wei, Suppress carrier recombination by introducing defects: The case of Si solar cell, *Appl. Phys. Lett.* **108** (2016) 022101.

[48] C. Messmer, M. Bivour, J. Schön, S.W. Glunz, M. Hermle, Efficient hole extraction for metal oxide based silicon heterojunction solar cells: A simulation study, *IEEE J. Photovolt.* **8** (2018) 456.

[49] Y.W. Chen, J.D. Prange, S. Dühnen, Y. Park, M. Gunji, C.E.D. Chidsey, P.C. McIntyre, Atomic layer-deposited tunnel oxide stabilizes silicon photoanodes for water oxidation, *Nature Mater*. **10** (2011) 539.

[50] S. Hu, M.R. Shaner, J.A. Beardslee, M. Lichterman, B.S. Brunschwig, N.S. Lewis, Amorphous TiO_2 coatings stabilize Si, GaAs, and GaP photoanodes for efficient water oxidation, *Science*, **344** (2014) 6187.

Figure captions

Figure 1. Growth rate per cycle (GPC) of the thermal- and plasma-ALD TiO_x films as a function of oxidation time (H_2O dose or O_2 plasma time) with different purge times (t_{purge}) after oxidation step. Inset shows the linear relationship between the TiO_x thickness and the number of ALD cycles for TiO_x films deposited under oxidation time of 6 s.

Figure 2. Effective minority carrier lifetime (τ_{eff}) curves as a function of excess carrier density for asymmetrically-passivated TiO_x/(*n*)c-Si/a-SiN_x:H stack, and symmetrically passivated a-SiN_x:H/(*n*)c-Si/a-SiN_x:H as a reference. TiO_x layers were deposited either by plasma- (red) or thermal-ALD (blue). Annealing was repeated at elevated temperatures in the ambient air. The solid line shows the theoretical limit imposed by Auger recombination. Inset shows the iV_{oc} versus annealing temperature.

Figure 3. (a) Schematic illustration of sample structures studied in this work. Throughout this study, *n*(*p*) and *N*(*P*) appeared in the figures indicate the carrier type of a-Si:H and c-Si, respectively. (b) Bar charts of external 1-sun V_{oc} in the initial (ini.) and after annealing (ann.) for four different solar cell structures shown in (a). Error bars indicate the spread of multiple measurement data for 1 or 2 samples. A 6-nm-thick TiO_x layer was deposited by either plasma- (red) or thermal-ALD (blue). Ti was used as a capping layer on top of the TiO_x. The results of the standard heterojunction solar cells (white) are also shown for comparison. The dashed lines show the iV_{oc} measured by QSSPC. The positive and negative external V_{oc} represent the magnitude of electron and hole selectivity, respectively.

Figure 4. Relationship between the work function of the capping metal or TCO contact and the external 1-sun V_{oc} of the two solar cell precursors with plasma-ALD TiO_x as electron contact (red) and thermal-ALD TiO_x as hole contact (blue).

Figure 5. External 1-sun V_{oc} as a function of TiO_x thickness. Plasma-ALD TiO_x/Al (red) and thermal-ALD TiO_x/ITO (blue) stacks were used for electron and hole contacts, respectively.

Figure 6. Impact of various plasma treatments (H_2, O_2 and Ar) of TiO_x layers on 1-sun external V_{oc} of the two solar cell precursors with (a) plasma-ALD TiO_x/Al as electron contact and (b) thermal-ALD TiO_x/ITO as hole contact. The positive and negative external V_{oc} represent the magnitude of electron and hole selectivity, respectively.

Figure 7. SPV signals (Φ) measured for TiO_x layers deposited on (a) *p*- and (b) *n*-type c-Si in the initial (ini.) and annealed (ann.) states. Error bars indicate the spread of multiple measurement data for 1 or 2 samples. TiO_x was deposited by plasma- (red) or thermal-ALD (blue). For comparison, SPV signals for a-Si:H *n* and *p* layers are also shown.

Figure 8. Capacitance-voltage measurements of GaIn/(*n*)c-Si/TiO_x/Al MIS structures for (a) plasma- and (b) thermal-ALD TiO_x, including simulated C-V curves to infer the concentration of charge in the TiO_x films from their flat-band shift.

Figure 9. V_{oc} of (a) *piNi*-x (x represents plasma/thermal-ALD TiO_x or *p*/*n* a-Si:H) and (b) *niNi*-x samples taken from the data in Figure 3b, plotted versus Φ measured on *P*/x and *N*/x contacts taken from the data in Figure 7, respectively. Similarly, the data are plotted for (*p*)c-Si base in (c) and (d). Open and closed symbols represent the initial and annealed states, respectively.

Figure 10. Possible band diagrams of the c-Si/(*i*)a-Si:H/TiO_x contact system explaining the inverse carrier selective behaviors observed in the plasma- (left) and thermal-ALD TiO_x (right). To highlight the role of the TiO_x layer, the contact systems with direct metal (TCO) contact are shown.